Available online at UofKEJ Website Here
UofKEJ Vol. 13 Issue 1 pp. 11-18 (July 2025)

UNIVERSITY OF KHARTOUM ENGINEERING JOURNAL (UofKEJ)

Performance of Thermal Power Plants in Tropical, Dry, Temperate, Continental, and Polar Climate Regions

Ali A. Rabah[1*], Mohamed Omer Sidahmed[2] and Asaad Y. Shamseldin[3]

[1]Department of Chemical Engineering, University of Khartoum, P.O. Box 321, Khartoum, Sudan.
[2]Water Research Center, University of Khartoum, P.O. Box 321, Khartoum, Sudan.
[3]Department of Civil and Environmental Engineering, University of Auckland, Auckland, New Zealand
[*]*Corresponding author (E-mail: rabahaa1967@gmail.com)*

ARTICLE INFO

Keywords:
tropical and dry climates, thermal power plants, efficiency, makeup water, and CO_2 emission.

Article History:
Received on: 16th May 2025
Accepted on :
Article Type:
Research Article

DOI: 10.5332/kuej.v13i1

ABSTRACT

The influence of climatic conditions on thermal power plant performance has been insufficiently addressed in existing research. This study investigates how different climate zones affect plant efficiency, resource use, and environmental impact. A 100 MW thermal power plant operating on the ideal Rankine cycle with superheat and reheat is used as a representative case study. Thirty years (1991–2021) of climate data from 92 global locations representing tropical, dry, temperate, continental, and polar regions are analyzed using Engineering Equation Solver (EES) software. Results show that tropical climates have ambient temperatures higher by 4°C, 10°C, 17°C, and 26°C compared to dry, temperate, continental, and polar regions, respectively. Plants in tropical and dry regions show a 1.0%–3.0% drop in efficiency, 12.0%–30.0% higher makeup water demand, 5.0%–11.0% greater cooling water needs, and 3.0%–6.5% increases in fuel consumption and CO_2 emissions. These outcomes highlight limitations and underscore the need for the importance of transitioning to renewable energy sources to enhance energy sustainability and water resilience.

Nomenclature

Roman letter		**Greek symbols**	
A	heat transfer area (m^2)	η	efficiency
C	heat capacity (W/K)	ε	effectiveness
cp	isobaric specific heat capacity (kJ/kg K)	φ	relative humidity (%)
h	enthalpy (kJ/kg)	ω	humidity ratio
LHV	lower heating value (MJ/kg)		
LG	liquid to gas ratio	a	air
M	mass flow rate (kg/s)	b	boiler
$\dot{M}$	mass flow rate (kg/s)	db	dry bulb
Me	Merkel number	f	fuel
MSE	mean square error	i	inlet
NTU	number of transfer units	g	generator
rms	root mean square error	max	maximum
P	electric power output	min	minimum
PE	percent error	o	outlet
$\dot{Q}$	heat transfer (W)	s	saturation
R	temperature range	th	thermal
T	temperature (°C)	w	water
U	overall heat transfer coefficient (W/m^2 K)	wb	wet bulb
$\dot{W}$	work (W)	$\dot{W}$	work (W)
x	quality	°	degree
y	variable		

1. INTRODUCTION

Thermal power plants are currently grappling with a multitude of challenges such as fossil fuel depletion, CO_2 emissions [1] water scarcity [2], [3], curtailment [4], and efficiency [5]. Despite these challenges, IEA [6] reported that "world electricity demand remained resilient in 2022; the electricity demand rose by 2% compared with 2.4% average growth rate seen over the period 2015-2019"; mostly covered by fossil oil based thermal power plants. Several factors contribute to this growth such as the global population,

industrialization, urbanization, energy security, geopolitical volatilities, and lifting of restrictive measures following the COVID-19 pandemic [22]. It is crucial to note that the latter three challenges viz water scarcity, curtailment, and efficiency are influenced by climatic conditions.

Macknick et al.[8] conducted a thorough review on water consumption in thermal power plants, rigorously comparing plants across various parameters, including technology (such as Generic, Steam, Combined Cycle, Subcritical, Supercritical, Integrated Coal Gasification Combined Cycle (IGCC)), cooling systems (once-through, cooling tower, and air cooling), and types of fuel (Nuclear, Natural Gas, Coal, Oil, Solar, Geothermal, and Biomass). However, they identified a research gap in comparing these plants based on their geographical location and climatic region. Although this gap was identified a decade ago, it continues to persist. Thermal power plants operating on the Rankine cycle typically consist of essential components: a boiler, turbine, condenser, and pump [9]. These plants utilize fuel to generate steam, which drives a turbine, producing mechanical work that powers an electric generator. The steam exiting the turbine is condensed and recirculated to the boiler. Condensation can be achieved using cold water derived from a cooling tower. The effectiveness of cooling towers is significantly influenced by climatic conditions such as temperature, humidity, and wind speed. Consequently, the performance of cooling towers has a substantial impact on key thermal power plant metrics, including efficiency, water and fuel demand, and CO_2 emissions.

Buryn et al. [10] conducted a study on the impact of weather conditions on the cooling tower of a 905 MW thermal power plant at the Opole Power Plant in Poland. They found that a 5°C increase in air temperature results in a 3-4°C rise in cooling water temperature, along with an increase in evaporation loss from 400-600 tons/h to 1000-1400 tons/h. Pattanayak et al. [11] examined the influence of cooling water on the steam surface condenser of a 210 MW thermal power plant with single reheat. Their study revealed that a 1°C change in cooling water temperature leads to a condenser pressure rise of 0.59 kPa, corresponding to a cycle heat rate deviation of 0.36% and a unit generation change of 33 MW.

Yuan et al. [12] investigated the cooling tower of a 300 MW thermal power plant. They found that at an ambient temperature of 30°C and a relative humidity of 40%, evaporation loss increases by 1.83%. However, at constant temperature, as relative humidity rises to 90%, the evaporation loss decreases to 1.1%, showing a linear decrease with humidity. Conversely, at constant relative humidity, evaporation loss increases linearly with temperature, with a rise of 26.65 tons/h of water for every 1°C increase in temperature. Similar findings were reported by Said et al. [7], and Coffel and Mankin [4].

Gao et al. [13] conducted a field test to investigate the impact of wind speed on a cooling tower at a 1.0 GW power plant. They concluded that wind speed has a negative effect on cooling water temperature. Specifically, at a wind speed of 4 m/s, the cooling water temperature difference drops by 15%. This negative impact of wind speed on cooling tower performance is also confirmed by studies conducted by Alavi et al. [14] and Lu et al [15].

This study focuses on key performance indicators such as cooling water temperature, water demand, power plant efficiency, fuel consumption, and CO_2 emissions. The study involves extensive climate data covering all climatic regions: tropical, dry, temperate, continental, and polar regions. The thermal power plant is simulated and energy and climate data are seamlessly integrated using Engineering Equations Solver (EES) software.

2. METHODOLOGY

A. Climate Data

Koeppen Geiger climate zone classification is considered [16]. A detailed description of the climate zones is provided in Table A.6 of the Appendix. Table A.1 to Table A.5 displays the considered locations spanning different climate zones. In total, there are 92 locations distributed among tropical (22), dry (26), temperate (22), continental (14), and polar (8) zones. It is important to note that the selection is based on climate data availability and representation of climates subgroups. The historical weather data (1991–2021) of the monthly average dry bulb or ambient temperature (T_a) and relative humidity φ for these 92 locations were extracted from the Climate Data website (https://en.climate-data.org).

B. Modelling of Rankine Cycle

Figure 1 presents a T-s diagram of a 100 MW thermal power plant operating on the ideal Rankine cycle with superheat and reheat principles, serving as a case study [9]. The cycle consists of four main components: a boiler, high- and low-pressure turbines, a condenser, and a feedwater pump. Steam lines are labeled 1 to 6. The energy balance for all units is established using the first law of thermodynamics under the following assumptions:

1. The boiler, turbine, and condenser in thermal power plants are typically insulated, leading to an assumption of adiabatic processes. Moreover, these plants operate with a constant steam flow rate, allowing us to consider the process as steady-state with minimal changes in kinetic and potential energy.
2. The condensate leaves the condenser as a saturated liquid (x=0), a typical condition in real life to prevent cavitation on the condensate pump.
3. For sub-zero temperatures the dry bulb is assumed as 0 °C; to avoid sub-zero cooling water temperatures
4. The plant is simulated using Rankine cycle under steady state conditions
5. The study is applicable to fuel oil power plants.

Superheat and Reheat (The plot is made using EES software)

Table 1 presents the energy balance of the Rankine cycle, while Table 2 lists the Rankine cycle, generator, and boiler efficiency. All symbols in the tables have usual meaning as listed in the nomenclature. The derivation of these equations is straightforward; however, more details are found in Moran and Shapiro [9]. An Engineering Equation Solver (EES) code has been developed based on the formulas provided in Table 1 and

Table 2. This code has been used to generate thermodynamic data for air, water, and steam and facilitate the calculation of the performance parameters.

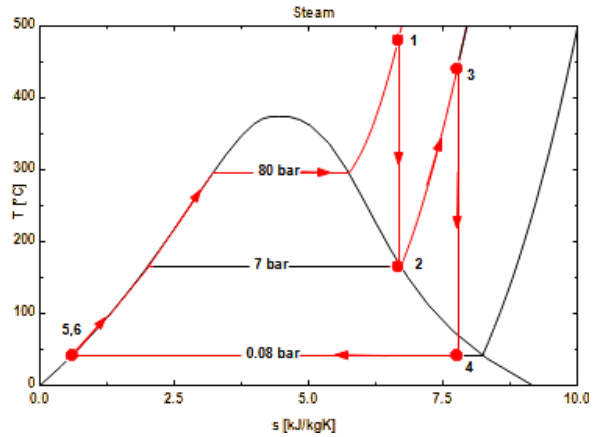

Figure 1: T-s diagram of Rankine Thermal Cycle with

Table 1: Rankine Cycle Energy Balance [9]

Units	Process	Parameter	Formula
Turbine 1	$1 \rightarrow 2$	Work output (W_{12})	$\dot{M}_s(h_1 - h_2)$
Boiler Reheat	$2 \rightarrow 3$	Energy input (Q_{23})	$\dot{M}_s(h_3 - h_2)$
Turbine 2	$3 \rightarrow 4$	Work output (W_{34})	$\dot{M}_s(h_3 - h_4)$
Condenser	$4 \rightarrow 5$	Energy removed (Q_{45})	$\dot{M}_s(h_4 - h_5)$
Feed water Pump	$5 \rightarrow 6$	Work input (W_{56})	$\dot{M}_s(h_6 - h_5)$
Boiler Superheat	$6 \rightarrow 1$	Energy input (Q_{61})	$\dot{M}_s(h_1 - h_6)$
Condenser	Water side	Energy removed (Q_W)	$\dot{M}_w c\, p_w(T_{wi} - T_{wo}$

Table 2: Thermal Power Plant Performance Parameters [9]

Performance Parameter	**Symbol**	**Formula**
Rankine Thermal Efficiency	η_{th}	$(\dot{W}_{12} + \dot{W}_{34} - \dot{W}_{56}) \div (\dot{Q}_{23} + \dot{Q}_{6}$
Generator Efficiency	η_g	$P_{el} \div (\dot{W}_{12} + \dot{W}_{34} - \dot{W}_{56})$
Boiler efficiency	η_b	$(\dot{Q}_{23} + \dot{Q}_{61}) \div M_f\, LHV$
Thermal Power Plant Efficiency	η_o	$\eta_{th}\eta_b\eta_g$

The condenser temperature is calculated using the effectiveness ε method as

$$\varepsilon = \frac{R}{T_c - T_{wi}} = 1 - e^{-NTU} \tag{1}$$

where $NTU = UA/C_{min}$ is the number of transfer unit, $R = T_{wi} - T_{wo}$ is the temperature range also coefficient of deprivation, C_{min} is the minimum heat capacity. Rearrangement of Equation (1) yields the condenser temperature as

$$T_c = T_{wi} - \frac{R}{\varepsilon} \tag{2}$$

C. Modelling of Cooling Tower

Cooling water temperature: The cooling water temperature T_{wi}, necessary for calculating the condenser temperature T_c, as per Equation (2) is determined through energy and material balance around the cooling tower [17], [18]

$$T_{wi} = T_{wo} - \frac{h(T_{ao}) - h(T_{ai})}{c\, p_w\, LG} \quad \text{where } LG = \frac{\dot{M}_w}{\dot{M}_a}, T_{ao} = \frac{(T_{wo} + T_{wi})}{2} \tag{3}$$

All symbols in Equation (3) have their standard meanings. LG is modelled using the following model [19] as

$$LG = \frac{NTU}{M\, e_M} \tag{4}$$

Merkel number M_{eM} is calculated using the procedure presented in Navarro et al. [18]. *MTU* and ε of the cooling tower are calculated using effectiveness method [20]

$$\varepsilon_t = \frac{\dot{Q}_a}{\dot{Q}_{max}} = \frac{1 - e^{-NTU(1-C^*)}}{1 - C^* e^{-NTU(1-C^*)}} \text{ where } C^* = \frac{C_{min}}{C_{max}} \tag{5}$$

$$\dot{Q}_a = \dot{M}_a\left[h(T_{ai}) - h(T_{ao})\right], \dot{Q}_{max} = C_{min}(T_c - T_{wi}) \tag{6}$$

Makeup water refers to the water added to the cooling tower basin to compensate for water lost due to evaporation (M_{ev}), drift (M_D), and blowdown (M_{BD}). Hence the make water, M_{makeup}, is estimated as the sum of the three losses [17]

$$\dot{M}_{makup} = \dot{M}_{ev} + \dot{M}_D + \dot{M}_{BD} \tag{7}$$

Evaporation loss is the difference between the moisture leaving and entering with ambient air. It can be determined from mass balance of the inlet and outlet air flow rate [21]

$$\dot{M}_{ev} = \dot{M}_w(\omega_o - \omega_i) \tag{8}$$

Drift loss is water loss due to entrainment. With the use of drift eliminated, the loss can be minimized within 0.2-0.5% of the total cooling water [10], [21]. A conservative estimate of the upper limit of 0.5 % is considered to cover a wide range of climatic regions [21]

$$\dot{M}_D = 0.005\, \dot{M}_w \tag{9}$$

Blowdown loss is the water that is drained from the cooling tower in order to avoid excessive mineral scale build-up and is estimated as [22]

$$\dot{M}_{BD} = \frac{\dot{M}_{ev}}{COC - 1} \tag{10}$$

where COC is the cycle of concentration, which is ratio of solid in cooling water to solid in makeup water. Pidaparti [21] limited COC to the range of 3 to 7. A value of 3 is used in this study for an upper estimate of blowdown.

3. RESULTS AND DISCUSSIONS

A. EES Code Validation

EES by F-Chart Software includes an extensive library of thermodynamic and transport properties for various substances, including water, steam, and air. It facilitates calculations for air's wet bulb temperature and humidity, steam's saturation pressure and enthalpy, as well as water's specific heat and enthalpy. Moreover, EES excels in solving thousands of coupled non-linear algebraic equations simultaneously, making it highly proficient for simulating thermal power plants. The accuracy of the EES model has been verified through a comprehensive comparison with the solved Example 8.3 of Moran and Shapiro [9], and with data from the cooling tower analysis conducted by Navarro et al. [18]. Figure 2 and Figure 3 show the validation results. Notably, the comparison yields an R^2 value of 1, indicating the model perfectly predicts the literature information. EES is used for both process simulation and data processing, including graphical presentations such as those shown in Figures 1 and 7. However, EES has a limitation in the graphical presentation of the T-s diagram (see Figure 1): the isobar lines in the liquid region overlap the saturation line.

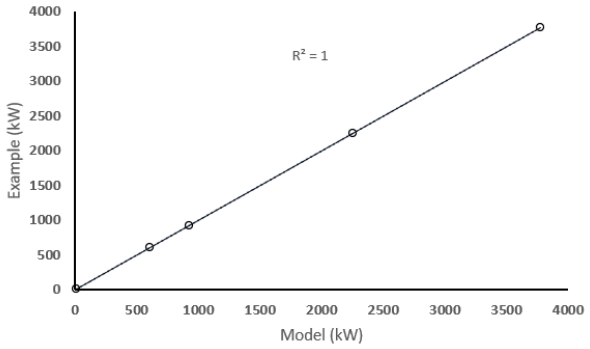

Figure 2: Rankine Cycle [9]

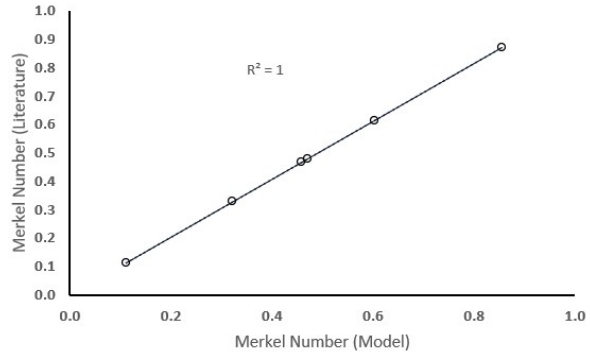

Figure 3: Merkel Number [18]

B. Climate Data Analysis

Figure 4 shows ambient temperatures for selected locations across five climate zones. Except for the tropical zone, all exhibit a sinusoidal annual trend. The tropical climate (Kampala) maintains a nearly constant temperature around 21°C. The figure also highlights significant temperature differences across zones. Figure 5 presents average ambient relative humidity (φ), with tropical, temperate, continental, and polar climates maintaining moderate to high levels (60–85%) year-round. In contrast, the dry climate (Riyadh) shows low humidity, typically below 25%. Figure A.1 summarizes the average temperature and humidity profiles, showing significant temperature variation across zones, while humidity remains fairly consistent—except in dry regions, which are distinctly arid.

Figure 6 illustrates the average ambient temperature per climate. In particular, the average ambient temperature of the tropical climate exceeds that of dry, temperate, continental, and polar climates by 4°C, 10°C, 17°C, and 26°C, respectively. These significant temperature differences are expected to have a notable impact on thermal power plant operating parameters. Figure 7 shows the average annual relative humidity for each climate. Tropical and polar exhibits relative humidity exceeding that of dry, temperature, and continental by 22%, 9% and 11% respectively.

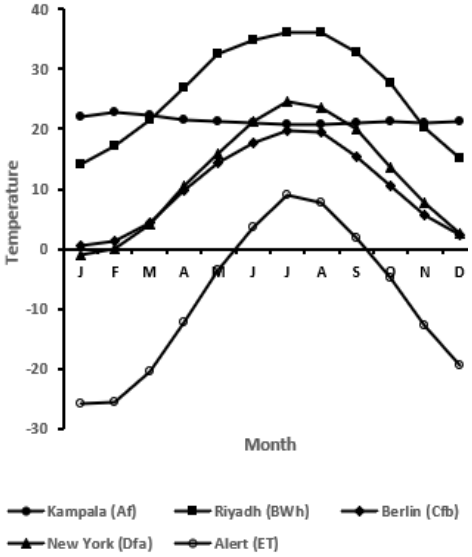

Figure 4: Profiles of Average Ambient Temperature [°C] Across Selected Locations

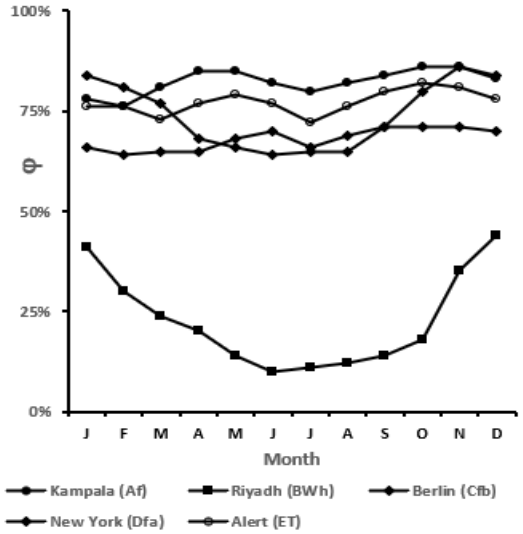

Figure 5: Profiles of Relative Humidly Across Selected Locations

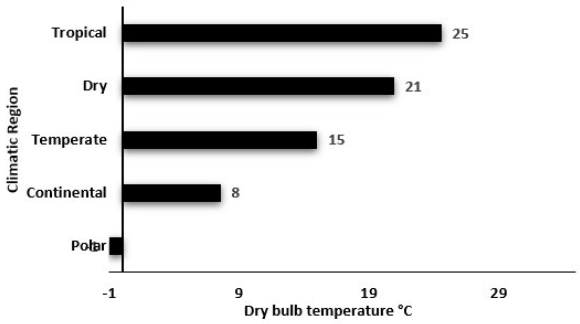

Figure 6: Average ambient temperature [°C] per climate

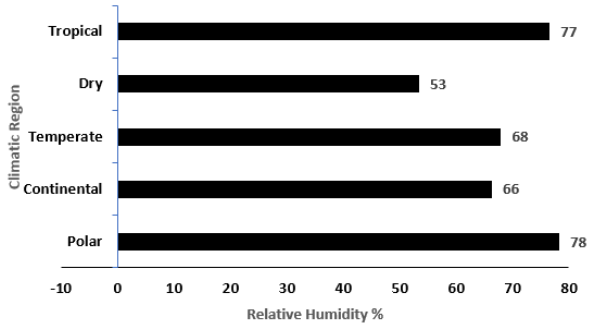

Figure 7: Average relative humidity [%] per climate

C. Cooling Water Temperature

Cooling water temperature is an important parameter in the assessment of the thermal power plant performance, it regulates the condenser vacuum pressure (P_s). Elevated cooling water (T_{wo}) leads to elevated P_s, resulting in reduced efficiency of the thermal power plant (η_o) and vice versa. T_{wo} is modelled as

$$T_{wo} = T_{wbi} + \Delta T_{approach} \quad (11)$$

where T_{wbi} is the air inlet wet bulb temperature and $\Delta T_{approach}$ is the approach temperature.

Figure 8 displays a 3D plot of ambient T_{ai}, φ_i and T_{wb}. In situations where sub-zero dry bulb temperatures (below 0°C) occur, the possibility of sub-zero cooling water temperatures arises. For instance, at a dry bulb temperature of 0°C, T_{wb} could reach approximately -6°C for all values of φ_i. To avoid sub-zero cooling water temperatures, a $\Delta T_{approach}$ of 7°C is adopted.

This precaution ensures that no T_{wo} falls below 0 °C, even during extreme cold conditions.

Figure 7 implies that $T_{wo} = f(T_{ai}, \varphi_i)$. Hence a multiple variables regression with a 99% confident limit is performed and the T_{wo} is

$$T_{wo} = -2.52 + 0.87\,T_{ai} + 11.64\,\varphi_i \quad (12)$$

Where T_{ai} in °C and φ_i in absolute value. The cooling water temperature gradient $\left(\frac{dT_{wo}}{dT_{ai}}\right)$ is 0.87, indicating that the cooling water temperature increases by 0.87°C for each 1°C rise in T_{ai} at constant relative humidity. Buryn et al. [10] observed that an increase in air temperature by 5°C (from 20–22°C to 25–27°C) results in a temperature rise at the outlet of the cooling tower by 3–4°C, a finding consistent with the results of this research.

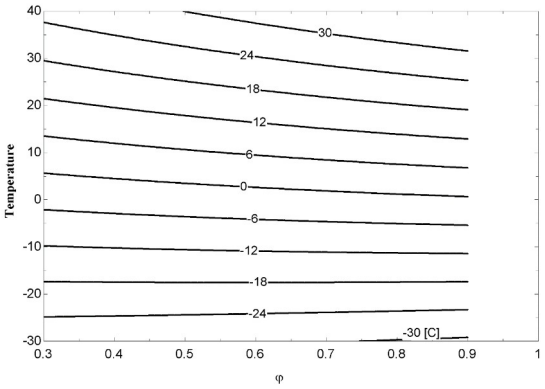

Figure 8: The isotherm lines of wet bulb temperatures in °C.

D. Condenser Vapor Pressure

Figure 9 shows the variation of condenser vapor pressure with cooling water temperature. The functional relation between P_s and T_{wo} assumes an exponential relationship.

$$P_s = 4.3584 \exp\left(0.0464\,T_{wo}\right) \quad (13)$$

where R^2 =0.9967

The pressure gradient ($\frac{dP_s}{dT_{wo}}$) at maximum temperature is 0.24-0.93 kPa/°C; meaning that for each 1 °C rise in T_{wo} the P_s rises by 0.24-0.93 kPa. Similar result is obtained by Pattanayak et al. [11], who obtained $P_s = 1.977 \exp\left(0.049\,T_{wo}\right)$ for T_{wo} range of 15 to 40°C.

Figure A.2 illustrates the impact of cooling water temperature on condenser temperature, with a noticeable decrease observed from tropical climates to polar climates. It is noteworthy that while dry climate experiences higher ambient temperatures compared to tropical climate, the latter typically exhibits higher relative humidity. Consequently, the cooling water temperature in tropical climates is higher than that in dry climate, as depicted in Figure A.2. The decrease in T_c enhances the efficiency of thermal power plants, as a lower condenser pressure enables the turbine to extract more energy from the steam. The condenser temperature is higher than cooling water temperature by 30°C.

E. Thermal Power Plant Efficiency

Figure 10 depicts the thermal efficiency plotted against condenser temperature. As the condenser temperature decreases, the lower pressure turbine extracts more energy from the steam, consequently increasing η_o. It is notable from Regression analysis that thermal efficiency decreases by 0.14% for every 1°C rise in T_c. Alternatively, in Figure 11, the thermal efficiency is plotted against ambient temperature, showing a decrease of 0.1% for every 1°C rise in ambient temperature. Attia [5] found that the thermal efficiency of the thermal power plant decreases by approximately 0.152% for every 1 °C increase in condenser temperature. Similar results are confirmed by Linnerud et al. [1] and Sanathara et al. [23].

Figure A.3 illustrates the variation in efficiency across different locations; the locations are ordered by climates. Efficiency generally improves as ambient temperature decreases; it increases as moving away from hot tropical and dry climates to cold polar climates. The colder climates of temperate, continental, and polar have a 1.0-3.0% advantage over tropical and dry climates in terms of thermal efficiency. This advantage is attributed to their cooler climate conditions, which promote more efficient operation

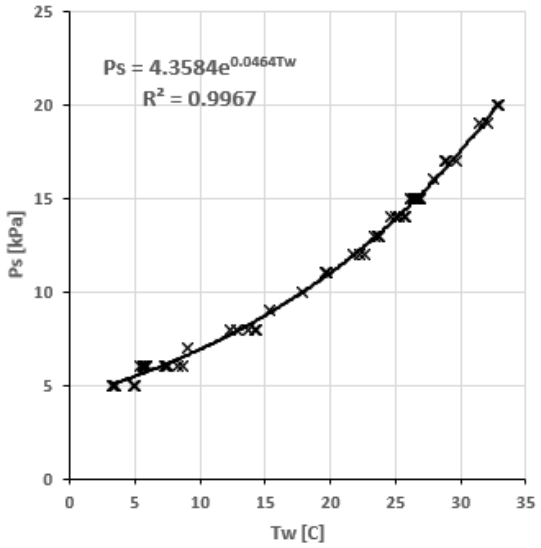

Figure 9: Impact of Cooling Water Temperature on Condenser Pressure

.

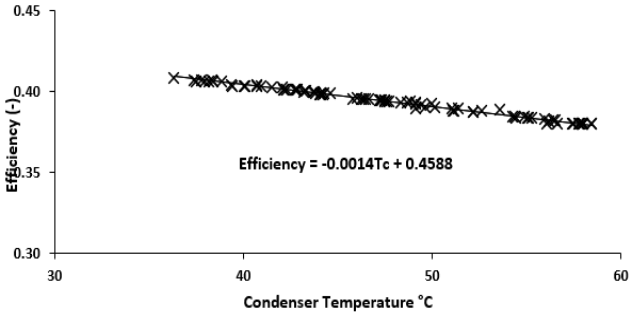

Figure 10: Efficiency vs Condenser Temperature

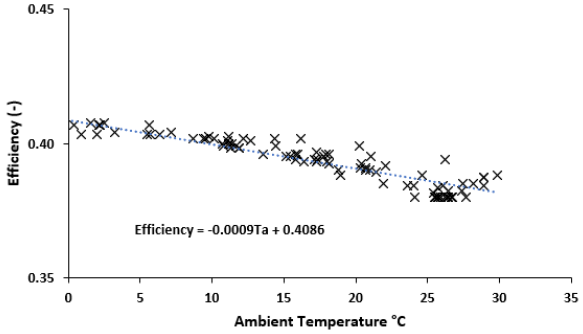

Figure 11: Efficiency vs Ambient Temperature

F. Makeup and Cooling Water Demand

Makeup water (M_{makeup}) and cooling water (M_w) demand are critical parameters for evaluating the performance of thermal power plants. Figure A.4 illustrates the profiles of M_{ev}, M_{BD}, M_D, M_{makeup}, and M_w for the considered locations. M_{ev} constitutes the major water loss, accounting for more than 70% of M_{makeup} and between 1.38% to 1.76 % of M_w. Makeup water constitutes 1.97% to 2.515 of cooling water demand. Yuan et al [12] indicated that M_{ev} represents 1.83% of M_w under conditions of air relative humidity (φ=40%) and ambient temperature at 30°C. As humidity increases, M_{ev} decreases to 1.1% of M_w at φ_i of 90%.

Figure 12 and Figure 13 display makeup water and water demand per climate. Notably, tropical and dry climates have the same order of magnitude for makeup water and cooling water. However, tropical and dry climates demand 12% to 30% more makeup water than other climates. Similarly, tropical and dry climates require 5% to 11% more cooling water demand than other climates. In dry climates, the high demand for makeup water coincides with significant challenges related to water scarcity and stress. Locations in dry climates, particularly those situated at the confluence of the African Sahara and Arabian Desert, face extremely high-water stress. Additionally, other regions such as East African countries are affected by water insecurity due to geopolitical tensions over the River Nile [23]. These factors raise concerns about the sustainability of thermal power plants in dry climates.

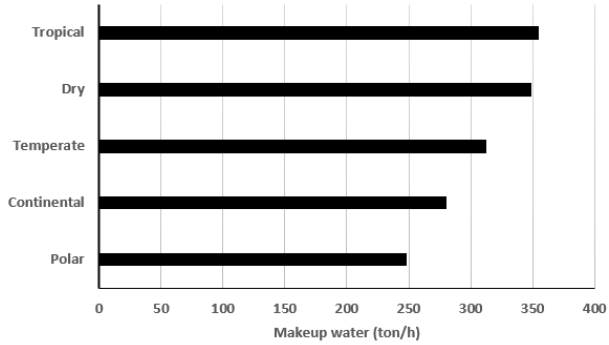

Figure 12: Makeup Water per Climate

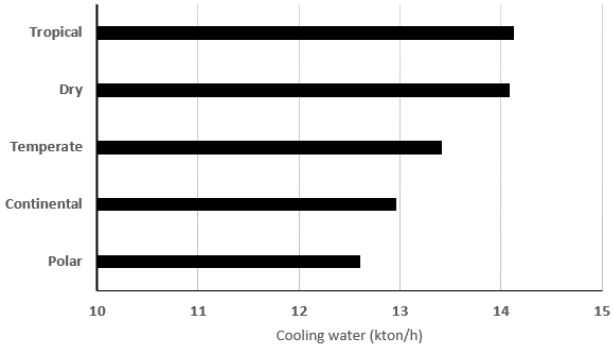

Figure 13: Cooling Water per Climate

G. Fuel Consumption and CO_2 Emission

The fuel utilized in this study is assumed to be Natural Gas (NG). A heating value of 45MJ/kg is considered, with

typical values ranging from 42-55 MJ/kg [24]. For our calculations, we also consider a conservative value of 80% for boiler efficiency, as typical boiler efficiencies range from 80-85% [25]. Regarding emissions, the emission factor for NG is calculated at 44 kg CO_2 per 16 kg of CH_4, resulting in 2.75 kg CO_2 per kg CH_4. These calculations are based on high-quality NG operating under complete combustion conditions, as represented by the Equation (14)

$$CH_4+2O_2=CO_2+2H_2O \quad (14)$$

Figure 14 and Figure 15 display fuel demand and its corresponding CO_2 emissions per location per climate type, respectively. Profile of fuel consumption for all locations are shown in Figure A.5. It is evident that temperate, continental, and polar climates exhibit 3.0% to 6.5% lower fuel consumption and CO_2 emissions compared to tropical and dry climates. In tropical and dry climates, the high fuel consumption and CO_2 emissions coincide with peak irradiance in these regions. Addressing the challenges of high fuel consumption and CO_2 emissions in tropical and dry climates could involve transitioning to abundant renewable energy sources [26]. Such a shift not only helps preserve finite resources but also significantly contributes to global efforts aimed at mitigating CO_2 emissions. Moreover, this transition aligns with the broader goal of reducing dependency on fossil fuels triggered by the projected decline in oil production. Adopting renewable energy sources enables societies to foster sustainable development while minimizing their environmental footprint.

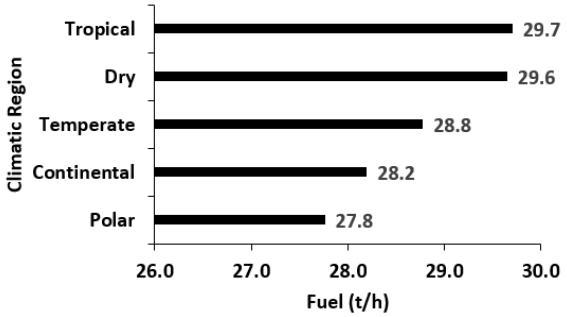

Figure 14: Fuel Consumption per Climate

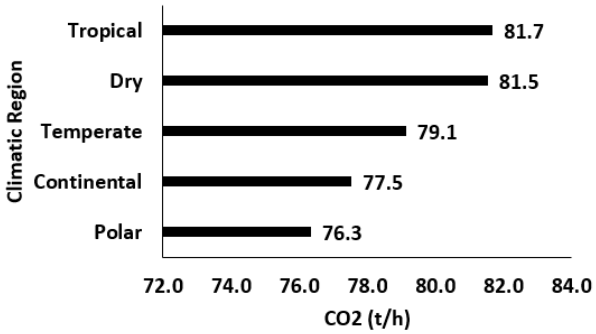

Figure 15: CO_2 Emissions per Climate

4. CONCLUSIONS

Locations within the same climate zone generally Have similar temperature and humidity levels, with exceptions noted. Certain areas within dry climate experience sub-zero temperatures, while coastal locations typically exhibit greater relative humidity than inland areas within the same zone. Ambient temperatures in tropical regions exceed those in dry, temperate, continental, and polar regions by approximately 4°C, 10°C, 17°C, and 26°C, respectively. Relative humidity levels do not significantly differ between tropical, temperate, continental, and polar climates, but dry climates generally have lower relative humidity compared to other climates.

For each 1°C rise in the ambient temperature at constant relative humidity the cooling water temperature increases by 0.87°C, condenser vapor pressure increases by 0.24-0.93 kPa and the thermal efficiency decreases by 0.152%.

The evaporation loss accounts for more than 70% of makeup water and between 1.38% to 1.76% of cooling water. Makeup water accounts for 1.97% to 2.51% of cooling water demand.

Tropical and dry climates:

a. water Requirements: makeup water 12%–30% higher
b. cooling water 5%–11% higher
c. fuel and Emissions: 3.0%–6.5% increase in fuel consumption and CO_2 emissions.
d. efficiency: lower by 1.0%–3.0%

The findings suggest that continued dependence on thermal power plants in tropical and dry climates presents challenges to both sustainability and reliability. Transitioning to renewable energy sources in these regions can reduce fossil fuel use, cut emissions, and enhance the resilience of water-stressed energy systems.

REFERENCES

[1]. Linnerud, K., Mideksa, T. K. & Eskeland, a. G. S., 2011. The Impact of Climate Change on Nuclear Power Supply. *The Energy Journal,* 32(1), pp. 149-168.

[2]. Schulze, C., Raabe, B., Herrmann, C. & S. Thiede, 2018. Environmental Impacts of Cooling Tower Operations – The Influence of Regional Conditions on Energy and Water Demands. *Procedia CIRP,* Volume 69, pp. 277-282.

[3]. Ibrahim, S., Ibrahim, M. & Attia, S. I., 2014. The Impact of Climate Changes on the Thermal Performance of a Proposed Pressurized Water Reactor: Nuclear-Power Plant. *International Journal of Nuclear Energy,* Volume 3, pp. 1-7.

[4]. Coffel, E. & Mankin, J., 2021. Thermal power generation is disadvantaged in a warming world. *Environental Research Letter ,* 16(2), pp. 1-11.

[5]. Attia, S., 2015. The influence of condenser cooling water temperature on the thermal efficiency of a nuclear power plant. *Annals of Nuclear Energy,* Volume 80, pp. 371-378.

[6]. IEA, 2023. *World Energy Inverstment,* s.l.: INTERNATIONAL ENERGY AGENCY.

[7]. IEA, 2022. *Real-Time Electricity Tracker,* Paris: World Energy Investment.

[8]. Macknick, J., Newmark, R., Heath, G. & Hallett, K., 2012. A Review of Operational Water Consumption and Withdrawal Factors for Electricity Generating Technologies. *Environmental Research Letter,* 303(4), pp. 275-300.

[9]. Moran, M. & Shapiro, H., 2006. *Fundamentals of Engineering Thermo-*. 5th Edition ed. Chichester: John Wiley & Sons, Inc.

[10]. Buryn, Z. et al., 2021. Impact of Weather Conditions on the Operation of Power Unit Cooling Towers 905 MWe. *Energies,* 14(19), pp. 1-19.

[11]. Pattanayak, L., Padhi, B. & Kodamasingh, B., 2019. Thermal performance assessment of steam surface condenser. *Case Studies in Thermal Engineering,* Volume 14, p. 100484.

[12]. Yuan, W. et al., 2020. The Effect of Air Parameters on the Evaporation Loss in a Natural Draft Counter-Flow Wet Cooling Tower. *Energies,* 13(23), p. 6174.

[13]. Gao, M., Zou, J., He, S. & Sun, F., 2018. Thermal performance analysis for high level water collecting wet cooling tower under crosswind conditions. *Applied Thermal Engineering,* Volume 136, p. 568–575.

[14]. Alavi, R. & Rahmati, M., 2016. Experimental investigation on thermal performance of natural draft wet cooling towers employing an innovative wind-creator setup. *Energy Conversion and Management,* Volume 122, pp. 504-514.

[15]. Lu, Y. et al., 2015. Experimental study of crosswind effects on the performance of small cylindrical natural draft dry cooling towers. *Energy Conversion and Management,* Volume 91 , pp. 238-248.

[16]. Kottek, M. et al., 2006. World Map of the Köppen-Geiger climate classification updated. *Meteorologische Zeitschrift,* 15(3), pp. 259-263.

[17]. Leeper, S., 1981. *Wet Cooling Towers: Rule-of-Thumb Design and Simulation. No.,* Idaho Falls, USA: EGG-GTH-5775. EG and G Idaho, Inc.

[18]. Navarro, P. et al., 2022. Critical evaluation of the thermal performance analysis of a new cooling tower prototype. *Applied Thermal Engineering,* Volume 213, p. 118719.

[19]. Jin, G.-Y.et al., 2017. A simplified modeling of mechanical cooling tower for control and optimization of HVAC systems. *Energy Conversion and Management,* Volume 48, pp. 355-365.

[20]. Rabah, A., 2023. *Heat transfer-Detailed Approach.* 1 ed. Khartoum: Khartoum University Press.

[21]. Pidaparti, S., Moisseytsev, A., Sienicki, J. & Ranjan, D., 2015. Counter flow induced draft cooling tower option for supercritical carbon dioxide Brayton cycle. *Nuclear Engineering and Design ,* 295(9), pp. 549-558.

[22]. Kroeger, D., 2004. *Air-Cooled Heat Exchangers and Cooling Towers: Thermal-Flow Performance Evaluation and Design.* s.l.:PennWell.

[23]. Matthews, R. & Vivoda, V., 2023. Water Wars': strategic implications of the grand Ethiopian Renaissance Dam. *Conflict, Security & Development,* 23(44).

[24]. WNE, 2023. *Annual report,* s.l.: World Nuclear Association

[25]. Ernest, A. & David, O., 2022. Boiler Efficiency Analysis of A 220mw Steam Power Plant Using Direct Method. *International Journal of Research and Scientific Innovation,* 9(8).

[26]. Abdelrazik, M., Abdelaziz, S., Hassan, M. & Hatem, T., 2022. Climate action: Prospects of solar energy in Africa. *Energy Reports,* Volume 8, pp. 11363-11377.